Respiratory rate estimation from multi-channel signals using auto-regulated adaptive extended Kalman filter ☆

Nishant Gupta [a,d], Patrizia Simmen [c], Daniel Trachsel [c], Andreas Haeberlin [d], Kerstin Jost [c,e], Thomas Niederhauser [a,b,*]

[a] Institute for Human Centered Engineering HuCE, Bern University of Applied Sciences, Bern, Switzerland
[b] sitem Center for Translational Medicine and Biomedical Entrepreneurship, University of Bern, Bern, Switzerland
[c] Department of Pediatrics, University Children's Hospital Basel UKBB, Basel, Switzerland
[d] Department of Cardiology, Bern University Hospital, University of Bern, Bern, Switzerland
[e] Department of Women's and Children's Health, Karolinska Institutet, Stockholm, Sweden

A R T I C L E   I N F O

A B S T R A C T

Background: Respiration rate (RR) is a major cause for false alarms in intensive care units (ICU) and is primarily impaired by the artifact prone signals from skin-attached electrodes. Catheter-integrated esophageal electrodes are an alternative source for multi-channel physiological signals from multiple organs such as the heart and the diaphragm. Nonlinear estimation and sensor fusion are promising techniques for extracting the respiratory activity from such multi-component signals, however, pathologic breathing patterns with rapid RR changes typically observed in patient populations such as premature infants, pose significant challenges.

Methods: We developed an auto-regulated adaptive extended Kalman filter (AA-EKF), which iteratively adapts the system model and the noise parameters based on the respiratory pattern. AA-EKF was tested on neonatal esophageal observations (NEO), and also on simulated multi-components signals created using waveforms in CapnoBase and ETNA databases.

Results: AA-EKF derived RR ($RR_{AA\text{-}EKF}$) from NEO had lower median (inter-quartile range) error of 0.1 (10.6) breaths per minute (bpm) compared to contemporary neonatal ICU monitors (RR_{NICU}): −3.8 (15.7) bpm (p < 0.001). $RR_{AA\text{-}EKF}$ error of −0.2 (3.2) bpm was achieved for ETNA wave forms and a bias (95% LOA) of 0.1 (−5.6, 5.9) in breath count. Mean absolute error (MAE) of $RR_{AA\text{-}EKF}$ with Capnobase waveforms, as median (inter-quartile range), at 0.3 (0.2) bpm was comparable to the literature reported values.

Discussion: The auto-regulated approach allows RR estimation on a broad set of clinical data without requiring extensive patient specific adjustments. Causality and fast response times of EKF based algorithms makes the AA-EKF suitable for bedside monitoring in the ICU setting.

1. Introduction

Respiratory rate (RR) is one of the critical vital signs that is continuously monitored in intensive care units (ICU) [1]. However, the accuracy of current state-of-the-art monitoring systems is limited by the artifact-prone signals acquired by indirect methods, such as impedance pneumography (IP) using skin-attached electrodes. In fact, continuously measured RR is considered a major cause for false alarms in ICU's leading to 'alarm fatigue' of caregivers [2,3]. Moreover, electrodes used in neonatal ICUs (NICU) can damage the fragile skin of neonates, particularly of preterm infants [4,5]. Additional challenge in tracking the RR in premature infants is posed by their immature respiratory

system, causing the RR to change rapidly [6–10]. Presence of cardiac activity in IP signals turns the detection of the respiratory components cumbersome, especially during bradycardia when the frequency spectrum of respiration- and cardiac-induced signals can overlap [11]. IP-based methods may also fail to recognize *post-sigh* small breaths leading to false negative apnea alarms [12].

Signals acquired using multiple electrodes integrated into an esophageal catheter is a potential alternative. Confined and intrinsically wet environment suppresses the electrode motion artifacts [13] and proximity to the heart and the diaphragm allows simultaneous acquisition of cardiac and respiratory signals [14], where the latter manifest

---

Fig. 1. **(a)** Overview of the AA-EKF approach. The algorithm uses all available knowledge about the system evolution that helps to isolate the individual signal components and estimate the $\omega_{activity}$. **(b)** Extended Kalman filter (EKF) based AA-EKF implementation for estimating the RR. The instantaneous cardiac frequency (ω_c) and baseline wander (**Y**) are *a priori* extracted using conventional methods (Section 2.2.2). The EKF estimates the states of a multi-component model (**X**$^+$, Sections 2.1.1 & 2.1.2). System knowledge is incorporated via the system model, known HR, adjustable noise parameters and adaptive regulation of state dynamics using the control parameters **u** (Section 2.2.3). Finally, the IF to RR block converts the estimated IF of the respiration (ω_r^+) to obtain the RR$_{AA\text{-}EKF}$ (Section 2.2.4).

as low-frequency baseline wander observed in distal electrodes [15]. However, RR estimation using existing algorithms have some key limitations. Algorithms based on respiratory modulations of the electrocardiogram (ECG) and/or the photoplethysmogram (PPG) [16] have limited applicability during fast breathing [17]. Similar to the IP-based signals, frequency based separation of the respiratory component in the baseline wander using fast Fourier transform or spectral analysis is also inadequate. Model based approaches using adaptive extended Kalman filters and smoothers for separating the components and fuse multiple signal sources [18–21] are promising, but have not been tested for tracking the fast varying neonatal RR.

In this work, we introduce an adaptive auto-regulated extended Kalman filter (AA-EKF) algorithm which estimates the respiratory frequency by optimally combining the information from multi-channel signals with empirical system knowledge. Similar to prior works [18, 19], AA-EKF uses a non-linear multi-component model to simultaneously track the respiratory and cardiac components, electrode motion artifacts, and additionally the instantaneous frequency (IF) of the respiration (hereafter denoted by $\omega_r = f_r/2\pi$ for simplicity). Whereas, adaptive auto-regulation limits the amplitude of individual components from erroneous over estimations, estimation of the ω_r as part of the EKF ensures fast tracking of the rapidly varying RR. We thereafter obtain the RR$_{AA\text{-}EKF}$ from ω_r and compare the estimation error (ΔRR$_{AA\text{-}EKF}$) with the errors by a modern neonatal intensive care unit (ΔRR$_{NICU}$) monitor. We further compare the AA-EKF estimated RR with standard RR estimation techniques using publicly available CapnoBase [22] and ETNA [23] databases, thus covering cardio-respiratory signals from patients of various age groups.

2. Materials and methods

2.1. Theoretical framework

2.1.1. System model for multi-channel respiratory signals

At the system level (Fig. 1a), the AA-EKF algorithm separates an oscillatory disturbance, for which only the frequency ($\omega_{disturbance}$) is available, and non-oscillatory, i.e. random interferences, from the desired quasi-periodic signal(s) of interest. Estimating a common $\omega_{activity}$ for multiple recording channels involves channel fusion. Both, the separation and fusion steps are main parts of the EKF framework.

In line with the above concept, we define a state-space model containing three components: cardiac (c), respiratory (r), and time-varying offsets (o) (including motion artifacts). The state-space incorporates these components as analytic signals [24,25] denoted by $X^{(I,Q)} \equiv \left[X^{(I)}, X^{(Q)}\right]$, where I and Q represent the in-phase and quadrature subcomponents, respectively. The state space also includes ω_r. Thus, for

N channels we write the complete state vector (**X**), the measurement vector (**Y**), and the state dynamics ($\dot{\mathbf{X}}$) as:

$$\mathbf{X}^{N'\times 1} = \begin{bmatrix} X_{c_i}^{(I,Q)} & X_{r_i}^{(I,Q)} & X_{o_i}^{(I,Q)} & \omega_r \end{bmatrix}^T \tag{1a}$$

$$\mathbf{Y}^{2N\times 1} = X_{c_i}^{(I,Q)} + X_{r_i}^{(I,Q)} + X_{o_i}^{(I,Q)} \equiv Y_i^{(I,Q)} \tag{1b}$$

$$\dot{\mathbf{X}}^{N'\times 1} = \begin{bmatrix} \dot{X}_{c_i}^{(I,Q)} & \dot{X}_{r_i}^{(I,Q)} & \dot{X}_{o_i}^{(I,Q)} & \dot{\omega}_r \end{bmatrix}^T \tag{1c}$$

where i represents the channel index with $1 \le i \le N$ and $N' = 6N + 1$ the total number of states. The measurement vector $\mathbf{Y}^{2N\times 1}$, which is the superposition of the three components, is also defined as an analytic signal with $Y_i^{(I)}$ being the baseline wander and $Y_i^{(Q)}$ being its Hilbert transform. The components of $\dot{\mathbf{X}}$ are defined as follows:

$$\begin{bmatrix} \dot{X}_{c_i}^{(I)} \\ \dot{X}_{c_i}^{(Q)} \end{bmatrix} = \begin{bmatrix} -\lambda_{c_i} & -\omega_c \\ \omega_c & -\lambda_{c_i} \end{bmatrix} \begin{bmatrix} X_{c_i}^{(I)} \\ X_{c_i}^{(Q)} \end{bmatrix} \tag{2a}$$

$$\begin{bmatrix} \dot{X}_{r_i}^{(I)} \\ \dot{X}_{r_i}^{(Q)} \end{bmatrix} = \begin{bmatrix} -\lambda_{r_i} & -\omega_r \\ \omega_r & -\lambda_{r_i} \end{bmatrix} \begin{bmatrix} X_{r_i}^{(I)} \\ X_{r_i}^{(Q)} \end{bmatrix} \tag{2b}$$

$$\begin{bmatrix} \dot{X}_{o_i}^{(I)} \\ \dot{X}_{o_i}^{(Q)} \end{bmatrix} = \begin{bmatrix} \lambda_{c_i} \cdot X_{c_i}^{(I)} + \lambda_{r_i} \cdot X_{r_i}^{(I)} \\ \lambda_{c_i} \cdot X_{c_i}^{(Q)} + \lambda_{r_i} \cdot X_{r_i}^{(Q)} \end{bmatrix} \tag{2c}$$

$$\dot{\omega}_r = -\lambda_{\omega_r} \cdot \omega_r \tag{2d}$$

Eqs. (2a) and (2b) model the cardiac and respiratory components as sinusoidal oscillations with instantaneous frequencies (ω_c and ω_r) and time-varying decay rates (λ_{c_i} and λ_{r_i}). Whereas ω_r is obtained directly from the state-space, ω_c is provided externally to the system model. Both frequencies are assumed to be similarly manifested in all N channels. Decay rates are used to apply constraints on the amplitudes of $X_{c_i}^{(I,Q)}$ and $X_{r_i}^{(I,Q)}$ and remove any offsets present in them. These offsets are tracked separately as $X_{o_i}^{(I,Q)}$ using Eq. (2c). Finally in (2d) we are assuming ω_r to be constant except for a decay. The role of decay rates is explained in Section 2.1.3.

2.1.2. State estimation using EKF

The extended Kalman filter is an iterative algorithm to optimally estimate the states of a non-linear system based on a predictive model and discrete observations. At each time step k of the EKF, the following *a-priori* (superscript -) estimates are first calculated:

$$\mathbf{X}_k^- = \phi\left(\mathbf{X}_{k-1}^+, \mathbf{u}_k\right) = \mathbf{X}_{k-1}^+ + \dot{\mathbf{X}}\left(\mathbf{X}_{k-1}^+, \mathbf{u}_k\right)\Delta t \tag{3a}$$

$$\mathbf{P}_k^- = \Phi_k \mathbf{P}_{k-1}^+ \Phi_k^T + \mathbf{Q}_k \tag{3b}$$

where $\mathbf{X}_{k-1}^+$ and $\mathbf{P}_{k-1}^+$ are the *corrected* (superscript +) state vector and error covariance matrix from the previous time step $k-1$, ϕ is the non-linear state transition function and Φ_k its *Jacobian* around $\mathbf{X}_{k-1}^+$, and $\mathbf{Q}_k$ is the covariance of the *process* noise. Thereafter, the Kalman gain

$\mathbf{K}_k$ is calculated and used to obtain the *corrected* state vector and error covariance estimates:

$$\mathbf{K}_k = \mathbf{P}_k^- \mathbf{H}_k^T \left(\mathbf{H}_k \mathbf{P}_k^- \mathbf{H}_k^T + \mathbf{R}_k \right)^{-1} \tag{4}$$

$$\mathbf{X}_k^+ = \mathbf{X}_k^- + \mathbf{K}_k \left[\mathbf{Y}_k - h\left(\mathbf{X}_k^-\right) \right] \tag{5a}$$

$$\mathbf{P}_k^+ = \left(\mathbf{I} - \mathbf{K}_k \mathbf{\Phi}_k \right) \mathbf{P}_k^- \tag{5b}$$

where h is the measurement function (same as Eq. (1b)) and $\mathbf{H}_k$ its *Jacobian*, and $\mathbf{R}_k$ is the covariance of the *measurement* noise.

To complete the system definition, we present here the principle structure of the process and measurement noises, with the exact definitions provided in subsequent sections.

$$\mathbf{Q}_k^{N' \times N'} = \mathrm{diag}\left(\begin{bmatrix} Q_{c_i,k} & Q_{c_i,k} & Q_{r_i,k} & Q_{r_i,k} & \cdots \\ & Q_{o_i,k} & Q_{o_i,k} & Q_{\omega_r,k} \end{bmatrix} \right) \tag{6a}$$

$$\mathbf{R}_k^{2N \times 2N} = \mathrm{diag}\left(\begin{bmatrix} R_{i,k} & R_{i,k} \end{bmatrix} \right) \tag{6b}$$

with $1 \le i \le N$. For both noise processes, $\mathbf{Q}_k$ and $\mathbf{R}_k$, zero cross-correlations and same values for the in-phase and quadrature sub-components for a particular analytic signal is assumed.

2.1.3. Auto-regulated adaptive EKF

In adaptive EKF, state estimation can be influenced by varying the functions ϕ and h, and the matrices $\mathbf{Q}_k$ and $\mathbf{R}_k$ at each iteration. In the proposed method, we exploit the property of an analytic signal to obtain the instantaneous amplitudes using:

$$A_{*,k}^+ = \sqrt{(X_{*,k}^{+(I)})^2 + (X_{*,k}^{+(Q)})^2} \tag{7}$$

at each iteration for the cardiac and respiratory components and incorporate them into the control vector $\mathbf{u}$ of the EKF algorithm. Thereafter, the state dynamics and the noise parameters are adapted based on empirical knowledge derived from these amplitudes.

State dynamics and decay rates: For small Δt, we can assume that the EKF iteration (Section 2.1.2) should not considerably alter $A_{c_i,k}^+$ or $A_{r_i,k}^+$. Thus, if a large increase in either is observed it can be considered as an overestimation. The decay rates, $\lambda_{c_i,k}$ and $\lambda_{r_i,k}$ respectively, can then be altered to selectively influence the *dampness* and control subsequent estimations. This phenomenon is based on the fact that for time-invariant ω and λ the analytic signal dynamical system is similar to a damped oscillator with $\lambda = \zeta \cdot \omega_n$ and $\omega = \omega_n \cdot \sqrt{1 - \zeta^2}$, where ω_n and ζ are the natural frequency and the damping constant, respectively (further details are provided in Supplementary Material). Furthermore, we use logistic function L of the form:

$$L\left(x_k, x_0, \Delta x \right) = \left[1 + \exp\left(-\frac{x_k - x_0}{\Delta x} \right) \right]^{-1} \tag{8}$$

where $x \in \mathbb{R}$ is an estimated quantity, x_0 is a threshold and Δx is a smoothing parameter to define such amplitude dependent decay rate. Compared to conditional functions, logistic transitions not only have lower impact on system linearity but also keep the decay rates differentiable with respect to $\mathbf{X}_k$ for the calculation of the *Jacobian* $\mathbf{\Phi}_k$.

Kalman Gain and Noise parameters: The underlying principle for setting the noise parameters $\mathbf{Q}_k$ and $\mathbf{R}_k$ is that they represent the *trust* in the predictive model and the measurements respectively and a higher Kalman gain ($\mathbf{K}_k$) favors the latter in state estimation. Generally, they are determined either from *a-priori* knowledge regarding the model/sensor errors or using empirical methods such as Monte Carlo simulations. However, given the dynamicity and complexity of both the system model and measurements, these methods are too cumbersome to be applicable for large number of patients or long measurement duration. Instead, in this work, we explore using the information gained from the amplitudes of estimated components as a feedback to suitably adjust the noise parameters in real-time. Specifically, setting the process noise for the cardiac and respiratory components proportional to

their respective amplitudes in each channel can facilitate signal separation. Similarly, setting the measurement noise (and thereby the influence of each channel on the ω_r^+) based on the respiratory component amplitude can facilitate channel fusion for frequency estimation.

The above relationship between the noise parameters and the state estimations of the proposed model can be better understood by analyzing the Kalman gain ($\mathbf{K}_k$) matrix elements for a simpler but analogous system. By setting:

$$N = 2, \quad X_{o_i,k}^{+(I,Q)} \equiv 0, \quad Q_{o_i,k} = 0$$

we can obtain the $\mathbf{K}_k$ for a 2-channel, 2-component system (excluding the time-varying offsets) by solving Eqs. (3a)–(4). Further simplifications ($P_{k-1}^+ \approx Q_k$ and small Δt), lead to following relationships between the elements of $\mathbf{K}_k$ (details are provided in the Supplementary Material):

$$\frac{\mathbf{K}_k \left\langle X_{r_i}^{(I)}, Y_i^{(I)} \right\rangle}{\mathbf{K}_k \left\langle X_{c_i}^{(I)}, Y_i^{(I)} \right\rangle} = \frac{\mathbf{K}_k \left\langle X_{r_i}^{(Q)}, Y_i^{(Q)} \right\rangle}{\mathbf{K}_k \left\langle X_{c_i}^{(Q)}, Y_i^{(Q)} \right\rangle} = \frac{Q_{r_i,k}}{Q_{c_i,k}} \tag{9a}$$

$$\frac{\mathbf{K}_k \left\langle \omega_r, Y_1^{(I)} \right\rangle}{\mathbf{K}_k \left\langle \omega_r, Y_2^{(I)} \right\rangle} = \frac{X_{r_1,k}^{-(Q)} / (Q_{c_1,k} + Q_{r_1,k} + R_{1,k}/2)}{X_{r_2,k}^{-(Q)} / (Q_{c_2,k} + Q_{r_2,k} + R_{2,k}/2)} \tag{9b}$$

$$\mathbf{K}_k \left\langle \omega_r, Y_i^{(I,Q)} \right\rangle = -\frac{Q_{\omega,k} \, X_{r_i,k}^{-(Q,I)}}{2 \, (Q_{c_i,k} + Q_{r_i,k} + R_{i,k}/2)} \, \Delta t \tag{9c}$$

Eq. (9a), which describes the influence of $Y_{i,k}^{(I,Q)}$ on the components $\hat{X}_{r_i}^{(I,Q)}$ and $\hat{X}_{c_i}^{(I,Q)}$, indicates that the fidelity of the estimated components towards the measured data would follow the pattern of the respective process noise. Similarly, Eq. (9b) describes the relative influence of the two channels in estimating ω_r. Although the ratio depends on the estimated state and process noise values, the relative value of $R_{1,k}$ and $R_{2,k}$ influences the weights of the two channels, as well.

The value of $Q_{\omega_r,k}$ in Eq. (9c) sets the overall *trust* in the time-invariance of ω_r^+ (ignoring the controlled decay). Hence it can be kept higher if larger deviations are expected. Such deviations in ω_r^+ can occur not only for time-varying RR but also if the respiratory waveform is not strictly sinusoidal. The latter scenario can cause large intra-breath deviations in ω_r^+ even for stable RR.

The exact definitions implemented for the decay rates and noise parameters, which are based on the above principles, are provided in Section 2.2.3.

2.2. RR estimation from physiological signals

2.2.1. Databases and reference RR

The *Neonatal Esophageal Observations* (NEO) database consists of multichannel signals from nine neonates, without respiratory support during the time of the measurement, recorded using Edi catheters (MAQUET, Solna, Sweden). The routine monitoring data from the neonatal intensive care unit (henceforth called NICU), which included surface ECG and IP and oxygen saturation (SpO2), was acquired simultaneously. The neonates were part of a prospective single-center observational study, conducted at the University Children's Hospital Basel, Switzerland. Details of the study design, the custom NEO setup, the registration of NICU data and its synchronization with the NEO signals are given in [14,15]. In a total of 405.4 h of recorded data, 934 events of either bradycardia (HR < 80 bpm for > 5s) or hypoxia (oxygen saturation < 88% for > 5s duration) were found. Out of these, 100 events were chosen *randomly* without prior knowledge of the signal quality. Respiration peaks and troughs were manually annotated by an experienced clinician for segments spanning one minute before and after the event. The clinician also classified the segments into 'good', 'medium', and 'bad' signal categories based on the ease of annotation. The proposed algorithm, however, does not depend on the *a-priori* determined signal quality. Only three segments, in which a

valid ECG was not detected in any esophageal channel (possibly due to disconnection) were excluded. For annotating the respiration cycles, the multi-channel esophageal signals were preprocessed to remove power-line interference (notch 50 Hz, bandwidth 1.4 Hz). Annotations were performed using the channel with strongest respiratory component (determined visually), however other channels could have been considered as well for doubtful signals. The surface ECG and synchronized NICU respiration signal were also available to distinguish respiratory activity from cardiac motion, esophageal peristalsis, and catheter motion artifacts. Further details regarding the setup used for annotation and the performance of the RR_{AA-EKF} with varying signal quality is published separately in [15].

CapnoBase contains 8-minute recordings of the ECG, the PPG and the capnogram along with annotated respiration cycles for 42 patients [22]. This database was used since the capnogram, which measures carbon-dioxide concentration of expired air, is the gold standard for measuring the RR. A 'hybrid' signal combining the capnogram and the PPG signals to mimic multi-component nature was used to estimate the RR by the AA-EKF algorithm. The results were then compared with the benchmark RR provided with the database.

Evaluation of technologies of Neonates in Africa (ETNA) database contains publicly available capnogram and PPG signals of 28 Neonates, both acquired using approved devices (Masimo Rad-97 Pulse CO-Oximeter with NomoLine Capnography) [23]. Previously, neonatal respiratory rate variability has been assessed using 130 epochs of 60 s duration each [26]. Since only the raw data and epoch locations were available for our study, we manually annotated the respiration peaks in the capnograms to obtain the RR_{ref}. Furthermore, only 64 epochs in which both, capnogram and PPG signals could be identified in the raw data, were included for analysis. RR_{AA-EKF} was estimated from a 'hybrid' of the capnogram and the PPG signals in the 64 epochs and was compared against the reference RR derived from the annotations.

Reference RR (RR_{Ref}) for each of the above cases was calculated from the time difference between the manually annotated peaks as follows:

$$RR_{Ref}((t_j + t_{j+1})/2) = \frac{60 \text{ s}}{t_{j+1} - t_j} \text{ bpm,} \tag{10}$$

where t_j is the time location of jth peak. For NEO and CapnoBase databases, RR_{Ref} from the peaks and troughs were calculated separately and subsequently averaged.

2.2.2. Pre-processing

The 8-channel NEO signals (1200 Hz sampling frequency) were jointly pre-processed to extract the esophageal ECG (EECG) component using the Elgendi algorithm [14,27]. Subsequently the location and amplitude of each QRS complexes was extracted. The R-peak interval was used to derive the HR and the R-peak amplitude was used to normalize the esophageal signals. The multi-channel 'baseline' signals (esophageal signal — EECG) was further filtered using a finite impulse response low pass filter with upper cutoff frequency set at 50% higher than the maximum HR in the individual segment.

For the CapnoBase data, a hybrid signal was created by (first) normalizing the capnogram and PPG signal individually with respect to their standard deviation and (second) adding them in 1:0.25 ratio. A 5 Hz low-pass filter was applied to suppress very high frequencies. The preexisting HR available in the database was used instead of calculating it from the ECG.

For the ETNA data, a similar rule as above was used to create the hybrid signal. Furthermore the HR was derived from the PPG signals using the ATH beat detector [28]. The algorithm was adjusted for the faster HR of neonates.

For all three databases, the pre-processed signals were re-sampled at 100 Hz and a finite impulse response based Hilbert transform was applied to obtain the analytic signal $\mathbf{Y}$. The instantaneous cardiac frequency (ω_c) was calculated by a linear interpolation of the HR to have the same time axis as that of the measured signal. The unit of (ω_c) was converted from beats/minute (bpm) to rad/s, as well.

2.2.3. AA-EKF estimator implementation

The AA-EKF estimator was implemented in MATLAB R2020b (The MathWorks Inc., USA) based on the steps described in Section 2.1.2. The two primary behavioral determinants, i.e. the decay rates and the noise parameters, were defined such that certain signal patterns (presence of artifact, absence of respiration, etc.) are recognized and suitable modifications for subsequent estimations are made as per the principles described in Section 2.1.3.

Control parameters: The instantaneous amplitudes (see Eq. (7)) obtained from $X_{c_i,k-1}^{+(I,Q)}$ and $X_{r_i,k-1}^{+(I,Q)}$, and $\omega_{r,k-1}^+$ were used to calculate the following set of parameters:

$$u_{1_i,k} = \widetilde{A}_{c_i,k}^+ \qquad u_{2_i,k} = \widetilde{A}_{r_i,k}^+ \qquad u_{3,k} = \widetilde{\omega}_{r,k} \tag{11}$$

where,

$$\widetilde{x}_k^+ = (1-\beta)\widetilde{x}_{k-1}^+ + \beta x_{k-1}^+$$

is a leaky integrator with forgetting factor β. For $\widetilde{A}_{c_i}^+$ we chose a long β of 20s since the cardiac amplitude was not observed to vary rapidly at least in the proximal channels (where it is the dominant component). For $\widetilde{A}_{r_i,k}^+$ and $\widetilde{\omega}_{r,k}$, β is set at 1s to keep the algorithm rapidly adaptable. Leaky integrator not only was used to suppress the effect of erroneous estimations rather also simplified the calculation of the *Jacobian* of $\phi(\mathbf{X}_k, \mathbf{u}_k)$ since we can consider $\partial \mathbf{u}_k / \partial \mathbf{X}_k$ to be negligible for $\Delta t \ll \beta$.

Decay rates: In line with Section 2.1.3, the decay rates were defined as a combination of a relevant frequency/rate term and a state dependent damping term:

$$\lambda_{c_i,k} = \omega_{c,k} \cdot \left[0.1 + 0.9 \cdot L\left(A_{c_i,k}^+ / \widetilde{A}_{c_i,k}^+, 2, 0.2\right)\right] \tag{12a}$$

$$\lambda_{r_i,k} = \left(\lambda_r^{(min)} + \widetilde{\omega}_{r,k}\right) \cdot$$
$$\left[0.25 + 0.75 \cdot L\left(A_{r_i,k}^+ / \widetilde{A}_{r_i,k}^+, 2, 0.2\right)\right] \tag{12b}$$

$$\lambda_{\omega r,k} = \widetilde{\omega}_r \cdot L\left(\widetilde{A}_{r_m,k}^+ / \widetilde{A}_{c_m,k}^+, 0.2, -0.2\right) \tag{12c}$$

$$m = \arg\max_i(\widetilde{A}_{r_i,k}^+)$$

In Eqs. (12a) and (12b), the damping term is based on the ratio of current amplitude over the smoothed amplitude. To ensure that a small decay is always present for offset removal, some constants were added. The valued for $\lambda_r^{(min)}$ in Eq. (12b) was specified during initialization (described later in this section).

For the respiratory frequency, the decay rate (Eq. (12c)) is normally 0 except when the ratio $\widetilde{A}_{r_m}^+ / \widetilde{A}_{c_m}^+$ becomes smaller that 0.2 in the channel m with maximum $\widetilde{A}_{r_i,k}^+$. This helps in suppressing overestimation of ω_r in the cases where small and fast fluctuations can corrupt the respiratory component during an apnea.

Noise parameters: The process noise parameters were set as follows:

$$Q_{c_i}^{(I,Q)} = 0.5 \cdot \widetilde{A}_{c_i}^+ \qquad Q_{r_i}^{(I,Q)} = 0.5 \cdot \widetilde{A}_{r_i}^+$$
$$Q_{o_i}^{(I,Q)} = 0.05 \cdot \widetilde{A}_{r_i}^+ \qquad Q_{\omega r,k} = Q_{\omega r,0} \tag{13a}$$

As per Section 2.1.3, the values for $Q_{c_i}^{(I,Q)}$ and $Q_{r_i}^{(I,Q)}$ were scaled according to the cardiac and respiration amplitudes, respectively, for each channel. $Q_{o_i}^{(I,Q)}$ is set as a small fraction of the respiration amplitude, so that the offsets are less sensitive to the process estimation by EKF but rather to the decay process in the state dynamics. The value of $Q_{\omega r}$ is set as time-invariant and is specified during initialization.
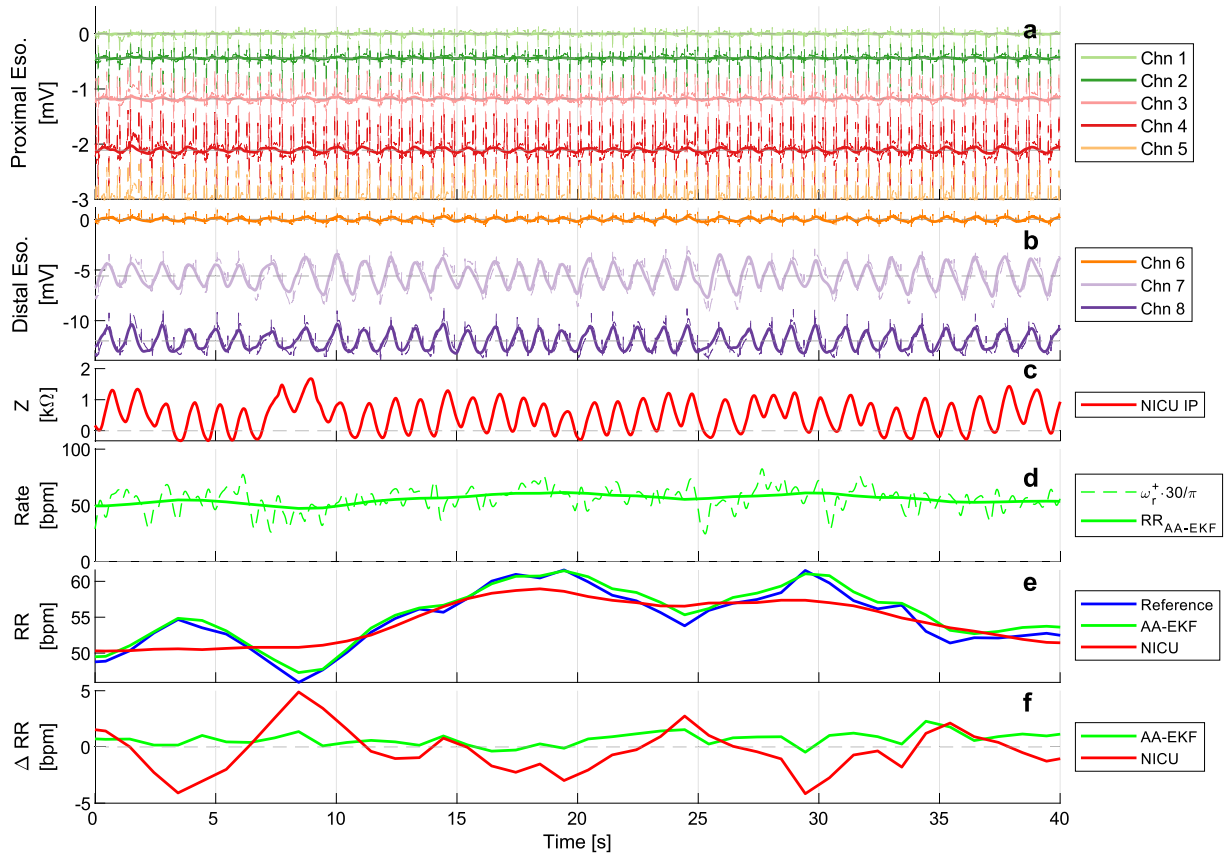
The measurement noise parameters were set as follows:

$$R_{i,k} = \left(\widetilde{A}_{r_i,k}^+ + \widetilde{A}_{c_i,k}^+\right) \cdot 10^{s_i} \tag{14}$$

where, $s_i = 1 - 2 \cdot L\left(\widetilde{A}_{r_i}^+ / \widetilde{A}_{c_i}^+, 2, 0.2\right)$

In the above, $\left(\widetilde{A}_{r_i}^+ + \widetilde{A}_{c_i}^+\right)$ sets the overall scale for the $R_{i,k}$ and $s_i \in [-1, \ 1]$ is a signal quality based non-linear weighting function [29] where the 'signal quality' is based on the relative values of $\widetilde{A}_{r_i}^+$ and $\widetilde{A}_{c_i}^+$.

Fig. 2. **(a,b)** Esophageal signals (ECG + respiration induced wander) derived from an infant of the NEO database breathing *regularly*; dashed lines — esophageal signals with strong influence from respiration activity, solid line — respiratory component estimated by the AA-EKF ($X_{r_i}^{(I)}$ in Eq. (1a)). **(c)** Synchronized IP signal from the NICU data showing similar respiratory waveform. **(d)** dashed lines — the instantaneous frequency of the respiratory waveform common to all the esophageal channels estimated by the EKF, solid line — the RR after post-processing ω_r^+. **(e)** RR from various methods. **(f)** RR difference w.r.t. the reference for the RR_{AA-EKF} and the RR_{NICU}.

Initialization: For all the segments in the NEO, the CapnoBase and the ETNA databases the value $\Delta t = 10$ ms was used. The state vector and the covariance matrix were initialized as follows:

$$X_{c_i,0}^{(I,Q)} = X_{r_i,0}^{(I,Q)} = \omega_{r,0} = 0 \, , \; X_{o_i,0}^{(I,Q)} = Y_{i,0}^{(I,Q)} \tag{15}$$

$$\mathbf{P_0}^{N' \times N'} = \mathbf{I}^{N' \times N'} \tag{16}$$

The control parameters were kept constant at $\widetilde{A}_{c_i}^+ = 1$, $\widetilde{A}_{r_i}^+ = 1$ and $\widetilde{\omega}_r = 2\lambda_r^{(min)}$ for the first 5 s of the EKF Loop. Thereafter, the next 5 s were used for stabilization. Hence, RR estimates from the first 10 s of measured data were discarded from comparison.

For the NEO and the ETNA signals $\lambda_r^{(min)} = 9$ bpm (0.2π rad/s), which is sufficiently lower than typical RR of neonates [17], and $Q_{\omega_r,0}$ = 16 was used. For the CapnoBase data $\lambda_r^{(min)}$ lowered to 0.1 bpm (0.03π rad/s) since fast breathing in resting conditions is typically observed in neonates, only. $Q_{\omega_r,0}$, however, was set at 64 since the respiratory waveform was observed to be less sinusoidal in shape leading to stronger intra-breath variations.

2.2.4. Post-processing: IF to RR

Physiological RR, which measures *complete* breaths per minute, was obtained after further processing ω_r^+. Instantaneous phase ϕ_r was calculated from ω_r^+ using trapezoidal integration. Time points at which $\phi_r(t)$ crossed the value of $2n\pi$ and $(2n + 1)\pi$ with $n = 1, 2, \ldots$ were defined as the positive and negative 'peaks' of a single respiration cycle respectively. A hysteresis of $\pi/2$ radians and minimum time interval of 1/3 s (180 bpm) was used to avoid unwanted crossings. Physiological RR was computed from these peaks based on their time intervals using (10). The total number of positive and negative peaks in an epoch were also counted and their minimum was defined the estimated number of complete breaths ($N_{breaths}$).

2.3. RR comparison

Accuracy of estimated RR was assessed based on two metrics, relative error (ΔRR) and the mean absolute error (MAE) define as:

$$\Delta RR_i = \hat{RR}_i - RR_{Ref,\, i}$$

$$MAE = \frac{1}{I} \sum_{i=1}^{I} |\Delta RR_i| \tag{17}$$

$\hat{RR}_i$ and $RR_{Ref,\, i}$ are the estimated and the reference RR averaged over a window i, and I is the total number of windows in the epoch. For this study, two window sizes, (1) 5s with 2s overlap and (2) 32s with 29s overlap were considered. The shorter window was needed to account for the fast changing RR (especially for neonates), while the larger enabled performance comparison with the earlier works [21,30,31].

For the ETNA database, we also computed the bias between the number of estimated (Section 2.2.4) and manually annotated breaths, and the 95% limits of agreement for comparison with the prior work [26].

For all statistical testing a sign test with $\alpha = 0.05$ was used.

3. Results

3.1. NEO signals

Figs. 2–5 illustrate the performance of AA-EKF algorithm on selected examples of the analyzed NEO signals. Figs. 2 and 3 are taken from measurements in which the respiration waveform is prominently present in the esophageal signals. Compared to RR_{NICU}, RR_{AA-EKF} manifests a higher bandwidth capable of tracking 'breath-to-breath' variability in RR. This is of significance particularly in cases of periodic
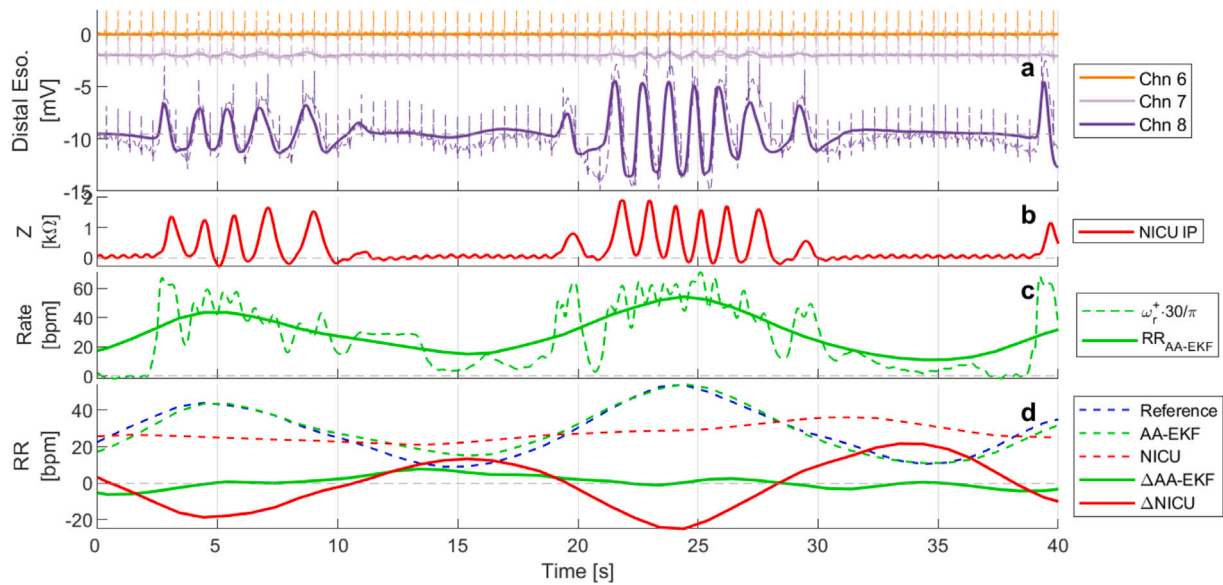
Fig. 3. (a) Esophageal signals from the distal channels derived from an infant of the NEO database showing periodic breathing; dashed lines — esophageal signals with strong influence from respiration activity but with short apneas ($\sim$ 5s) at around times 15s and 35s, solid line — respiratory component estimated by the AA-EKF ($X_{r_i}^{(I)}$ in Eq. (1a)). **(b)** Synchronized IP signal from the NICU data confirming the apneas in the same time period. **(c)** dashed line — the instantaneous frequency of the respiratory waveform common to all the NEO channels estimated by the EKF, solid lines — the RR after post-processing ω_r^+. **(d)** dashed lines — RR from various methods with the RR_{NICU} not showing signs of the periodic breathing, solid lines — RR difference w.r.t. the reference for the $RR_{AA\text{-}EKF}$ and the RR_{NICU}.
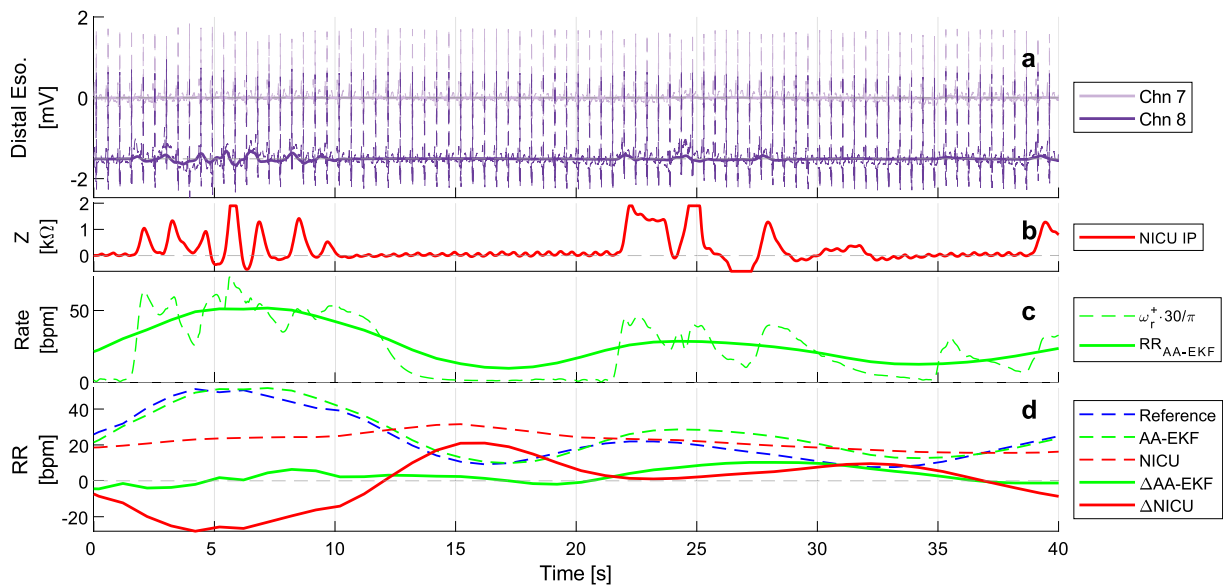
Fig. 4. (a) Esophageal signals from the distal channels derived from an infant of the NEO database showing episodes of periodic breathing; dashed lines — esophageal signals with *weak* influence from respiration activity and with short apneas at around times 15s and 35s, solid line — respiratory component estimated by the AA-EKF ($X_{r_i}^{(I)}$ in Eq. (1a)). **(b)** Synchronized IP signal from the NICU data confirming the apneas in the same time period. **(c)** dashed line — the instantaneous frequency of the respiratory waveform common to all the NEO channels estimated by the EKF, solid lines — the RR after post-processing ω_r^+. **(d)** dashed lines — RR from various methods with the RR from the NICU again not showing signs of the periodic breathing, solid lines — RR difference w.r.t. the reference for the $RR_{AA\text{-}EKF}$ and the RR_{NICU}.

breathing (Fig. 3) since the short apneas are not apparent from RR_{NICU} alone. Fig. 2 also includes the signals from proximal channels to illustrate the typical spatial distribution of the respiratory waveform. For the subsequent figures, the proximal channels are omitted.

In Fig. 4, none of the channels shows a strong respiration signal. The RR_{EKF} nevertheless managed to follow the reference RR, thanks to the good suppression of the cardiac oscillation in the estimated respiration waveform.

Fig. 5 depicts an example in which the amplitude of respiratory signal drops suddenly even though the IP (NICU) signal suggests that the actual apnea occurs only later. The drop in the respiration amplitude

could be the result of a displacement of the esophageal electrodes. However, thanks to the adaptability of the AA-EKF algorithm, significant errors in the estimated RR are avoided.

3.2. Simulated hybrid signals

Fig. 6 illustrates the performance of AA-EKF applied to a selected hybrid signal created from the CapnoBase dataset. Even though the respiratory waveform noticeably deviates from a sinusoidal signal, the estimated values are remain realistic. We can observe that instantaneous frequency is highly erratic, which is understandable since (a)
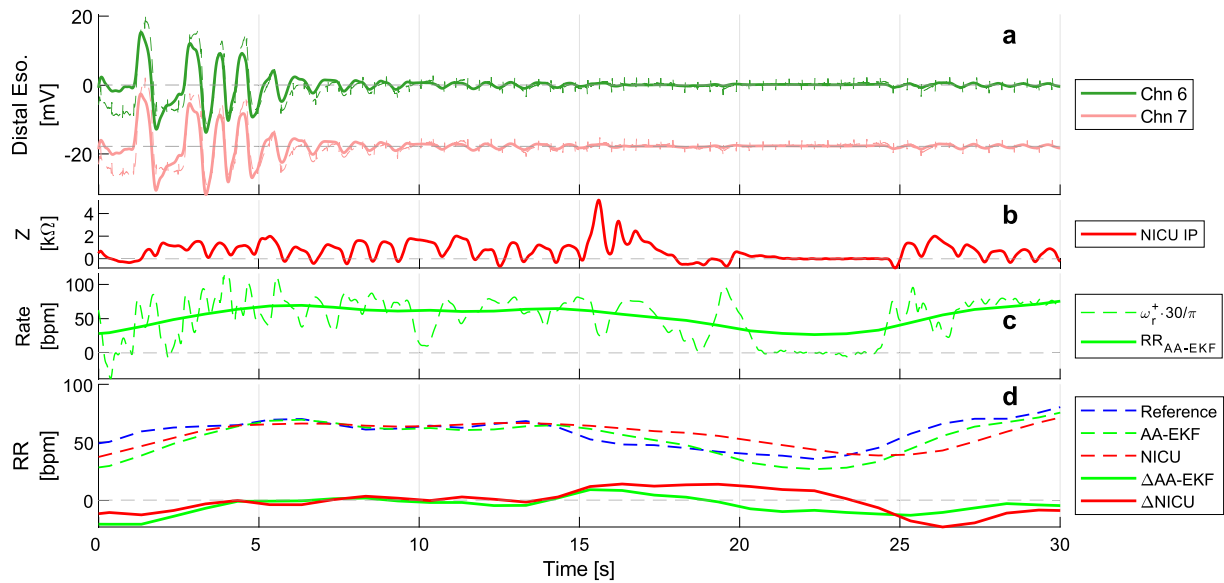
Fig. 5. **(a)** *Peculiar* esophageal signals from the distal channels derived from an infant of the NEO database prior to an apnea; dashed lines — esophageal signals with the influence from the respiration activity changing from strong (time< 5s) to weak (time=7.5s–15s) prior to an apnea, solid lines — respiratory component estimated by the AA-EKF ($X_{r_i}^{(I)}$ in Eq. (1a)). **(b)** Synchronized IP signal from the NICU data confirming the apneas around time=22.5s but without comparable prior drop in the signal amplitude. **(c)** dashed line — the instantaneous frequency of the respiratory waveform common to all the NEO channels estimated by the EKF, solid lines — the RR after post-processing ω_r^+ and becoming small only during the actual apnea. **(d)** dashed lines — RR from various methods with the RR from the NICU again not reacting fast enough to the apnea at time=22.5s, solid lines — difference from the reference RR for the RR from the NICU and the EKF algorithm.
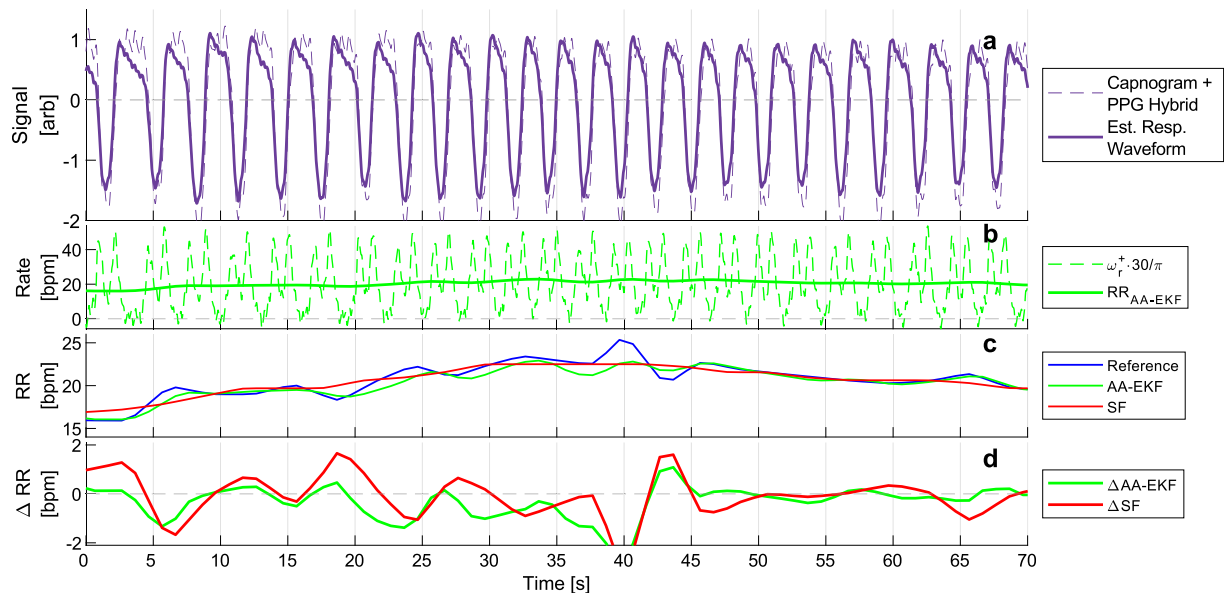
Fig. 6. **(a)** Performance of the EKF using the signals in the CapnoBase [22] database; dashed line — the 'hybrid' signal created using the capnogram and PPG signals from a *spontaneously* breathing patient; solid line — respiratory component estimated by the AA-EKF ($X_{r_i}^{(I)}$ in (1a)). **(b)** dashed line — the instantaneous frequency of the respiratory waveform estimated by the EKF showing separate inspiration and expiration peaks, solid lines — the RR after post-processing ω_r^+. **(d)** dashed lines — RR from various methods, solid lines — RR difference w.r.t. the reference for the SmartFusion (SF [32]) and the EKF.

the inspiration and expiration duration are not equal and (b) there exists short period in-between them with no airflow. However, the estimated RR is still accurate and stable thanks to the post processing steps (Section 2.2.4) .

RR$_{\text{AA-EKF}}$ showed similar performance when applied to hybrid signals from ETNA database. There too, the RR$_{\text{AA-EKF}}$ was able to closely follow the variations in the respiratory signal. An illustrative example can be found in Figure 2 of the Supplementary Materials.

3.3. RR comparison

Table 1 summarizes the errors in estimated RR with respect to the reference. For the NEO database and 5s window, we observe a lower IQR for ΔRR$_{\text{AA-EKF}}$ compared to ΔRR$_{\text{NICU}}$ which reflects the better tracking of rapidly changing RR. RR$_{\text{NICU}}$ also underestimated the RR by 3.8 bpm ($p < 0.001$). MAE of RR$_{\text{AA-EKF}}$ is 30% lower compared to RR$_{\text{NICU}}$ ($p < 0.001$) for 5s window and 20% lower ($p = 0.04$) for the 32s

Table 1

RR estimation error given as median (IQR) in breaths/minute for 5s and 32s window lengths.

Database	ΔRR		MAE	
Method	5s	32s	5s	32s
NEO:				
AA-EKF	0.1 (10.6)	0.1 (8.3)	6.9 (4.5)	4.7 (4.9)
NICU	−3.8 (15.7)	−4.0 (9)	10.0 (3.9)	5.9 (4.6)
CapnoBase:				
AA-EKF	−0.1 (0.4)	−0.1 (0.3)	0.3 (0.2)	0.3 (0.2)
ETNA:				
AA-EKF	−0.2 (3.2)	−0.6 (3.0)	2.6 (3.2)	1.7 (2.7)

NEO: Neonatal Esophageal Observations, NICU: Neonatal Intensive Care Unit, AA-EKF: Auto-regulated Adaptive Extended Kalman Filter (this work), ETNA: Evaluation of Technologies for Neonates in Africa.

Table 2

Comparison of AA-EKF with reported values in the literature for different methods.

CapnoBase	MAE$_{32s}$ median (IQR)
AA-EKF	0.3 (0.2) bpm
KS [21]	0.3 (0.5) bpm
ARM [30]	1.4 (2.8) bpm
SF [31]	1.1 (2.3) bpm
ETNA	N$_{breaths}$ bias (LOA)
AA-EKF	0.1 (−5.6, 5.9)
IMS [26]	−0.52 (−2.7, 1.66)

KS: Kalman Smoother, ARM: Auto-Regressive Modeling, SF: Smart Fusion, IMS: Incremental Merge Segmentation, LOA: 95% Limits of Agreement.

window. Results from CapnoBase database showed similar RR$_{AA-EKF}$ for both windows, which is in line with previously reported claims of 32s window being adequate. For the ETNA database ΔRR$_{AA-EKF}$ IQR and MAE were lower compared to NEO, which is most likely because the epochs in the ETNA database were pre-selected based on signal quality of the capnograms.

Table 2 provides the reported values for MAE of algorithms tested using CapnoBase dataset. It can be seen that the RR$_{AA-EKF}$ has a good accuracy, but, it need to be mentioned that it was derived from *simulated* multi-component signals rather than the ECG/PPG signals only. N$_{breaths}$ computed for ETNA signals also showed low bias from the manual breath counts, however, with a larger spread in the LOA compared to the reported value. This discrepancy could be due to small but consistent bias in ω_r^+ in some epochs leading to errors in N$_{breaths}$.

4. Discussion

Discerning the respiratory component from interference in the respiratory signals is a significant challenge in clinical routine such as intensive care. Non-linear adaptive filters, especially extended Kalman filters and smoothers, are promising since they enable processing of complex signals and combining multiple sources of information. However, slow adaptation speed is a key bottleneck for their application on signal exhibiting fast varying characteristics, such as the NEO signals, considered in this work.

The proposed AA-EKF algorithm extends the capabilities of previously developed techniques [18–21] by improving the adaption speed. Amplitude-based model dynamics and noise parameters ensure that the respiratory component remains distinguishable even with irregular breathing patterns and signal artifacts. Such cases are caused by both physiological (short apnea, periodic breathing, sighs, deep breathing) and technical (electrode contact) reasons. Another distinguishing aspect of this work is the direct estimation of respiratory frequency from multi-channel signals. In contrast, earlier approaches first estimate a fused respiratory signal and then use standard techniques, such as peak detection, for computing the RR and normally require a few cycles to improve accuracy. By circumventing this intermediate step, AA-EKF estimates the respiratory frequency (ω_r^+) with higher bandwidth. Our results indicate that RR estimated from the ω_r^+ is able to closely match the underlying respiratory pattern, however small biases can lead to errors in the total breath count.

Defining the rules for recognizing different respiratory patterns and suitably adapting subsequent estimations (Section 2.2.3), does require careful tailoring to attain accuracy and stability. Nevertheless, the applicability of the AA-EKF algorithm is widened and improvements in RR estimation is achieved without resorting to preclusions based on signal quality or requiring excessive *a priori* information. Hence, the model developed for neonatal respiratory pattern provided good estimation for both the NEO signals and multi-component signals simulated using ETNA database. Furthermore, only minor modifications ($\lambda_r^{(min)}$ and $Q_{r,0}$) were required to adapt the algorithm developed for neonatal respiratory patterns for the ones for older patients.

On the NEO database, AA-EKF performed significantly better than the standard monitoring device, especially for the 5s window, most likely due to lower errors during fast RR variations. However, the spread in Δ RR (10.6 bpm) and the MAE$_{5s}$ value (6.9 bpm) were considerable, due to the signals with low respiration quality. Catheter optimizations (e.g., electrode placement and number) may improve these numbers by increasing the chance for capturing respiratory signals.

Results with simulated signals derived from the CapnoBase and ETNA data-set show that the RR estimation is robust against the presence of cardiac components. Although the ratio of the respiratory and the cardiac component was fixed for each segment of the simulated signals, inherent variations in the instantaneous amplitudes were preserved. Additional scenarios, in which this ratio may be varied to further test the applicability of the model may be done in future studies but were beyond the scope of the present work.

The key assumptions regarding the signal characteristics in the rules for RR estimation is the dominance of respiratory component in at least one measured channel, the frequency of sustained inference (heart rate in this case) being known, and the other disturbances, which are modeled as time-varying offset at present, being short. These conditions can normally be expected for the bedside monitoring of resting patients. Sustained body movements and peristaltic motion (during feeding for example) may, however, lead to inaccurate and unstable estimation. The AA-EKF approach might still be feasible by further augmenting the system model to track these activity as well, but may require additional signal modalities such as accelerometer or pressure sensors. Multi-modal signal acquisition from soft and conformable sensor systems, either skin attached or catheter integrated, are still in the nascent stages of development.

Although AA-EKF was tested with pre-recorded signals so far, its main building blocks (see Fig. 1) are based on causal algorithms only that consequently allow for a real-time implementation. The EKF itself is causal (unlike the Kalman smoothers) and can provide estimates with a short delay using an appropriate choice of noise parameters. The post-processing stage is causal, as well. A new RR estimate becomes available at every phase crossing, however, it may be averaged over a few respiration cycles to improve the estimation accuracy. The pre-processing stage includes HR estimation and the Hilbert transform, both can be done with (a cascade) of linear filters providing real time implementation capability [33,34].

EKF based algorithms may nevertheless pose challenges for real-time applications due to the matrix inversions involved. The computational complexity typically scales with $\mathcal{O}(N^3)$, N being the number of states. However, EKF based algorithms have recently been implemented in low-cost wearable devices such as real-time body position monitor [35] and gait monitoring [36]. Although N used for the proposed AA-EKF was considerably higher due to the number of channels involved, a bedside ICU monitor show less power constraints than wearables. In addition, N could be reduced by restricting the number of tracked channels iteratively based on knowledge of previous estimates.

5. Conclusion

Auto-regulated adaptive EKF allows tracking of fast changing respiratory signals and the RR even with interferences from cardiac activity and motion artifacts. AA-EKF is able to incorporate multi-channel information and empirical knowledge of the signal characteristics to improve estimation accuracy. With further improvements, such as inclusion of multiple signal modalities and automated patient specific optimization, RR estimation may become a reliable monitoring tool even for acute situations in the intensive care setting.

CRediT authorship contribution statement

Nishant Gupta: Conceptualization, Methodology, Software, Validation, Investigation, Formal analysis, Resources, Data curation, Writing – original draft, Writing – review & editing, Visualization. **Patrizia Simmen:** Investigation, Data curation. **Daniel Trachsel:** Investigation, Data curation. **Andreas Haeberlin:** Supervision, Writing – original draft, Writing – review & editing. **Kerstin Jost:** Formal analysis, Investigation, Resources, Writing – original draft, Writing – review & editing. **Thomas Niederhauser:** Supervision, Writing – original draft, Writing – review & editing, Project administration, Funding acquisition.

Declaration of competing interest

The authors declare that they have no known competing financial interests or personal relationships that could have appeared to influence the work reported in this paper.

Data availability

Data will be made available on request.

Appendix A. Supplementary data

Supplementary material related to this article can be found online at https://doi.org/10.1016/j.bspc.2023.104977.

References

[1] N. Kumar, G. Akangire, B. Sullivan, K. Fairchild, V. Sampath, Continuous vital sign analysis for predicting and preventing neonatal diseases in the twenty-first century: big data to the forefront, Pediatr. Res. 87 (2019) 210–220, http://dx.doi.org/10.1038/s41390-019-0527-0, 2019 87:2.

[2] F. Dursun Ergezen, E. Kol, Nurses' responses to monitor alarms in an intensive care unit: An observational study, Intensive Crit. Care Nurs. 59 (2020) 102845, http://dx.doi.org/10.1016/j.iccn.2020.102845.

[3] A.-S. Poncette, C. Spies, L. Mosch, M. Schieler, S. Weber-Carstens, H. Krampe, F. Balzer, Clinical Requirements of Future Patient Monitoring in the Intensive Care Unit: Qualitative Study, JMIR Med. Inform. 7 (2) (2019) e13064, http://dx.doi.org/10.2196/13064.

[4] M. Barak, S. Hershkowitz, R. Rod, S. Dror, The use of a synthetic skin covering as a protective layer in the daily care of low birth weight infants, Eur. J. Pediatr. 148 (7) (1989) 665–666, http://dx.doi.org/10.1007/BF00441529.

[5] J.H. Behr, D. Wardell, C.L. Rozmus, R.L. Casarez, Prevention strategies for neonatal skin injury in the NICU, Neonatal Netw. 39 (2020) 321–329, http://dx.doi.org/10.1891/0730-0832/11-T-623.

[6] D. Holditch-Davis, M. Scher, T. Schwartz, Respiratory development in preterm infants, J. Perinatol. 24 (2004) 631–639, http://dx.doi.org/10.1038/sj.jp.7211150.

[7] A.B. te Pas, C. Wong, C.O.F. Kamlin, J.A. Dawson, C.J. Morley, P.G. Davis, Breathing patterns in preterm and term infants immediately after birth, Pediatr. Res. 65 (2009) 352–356, http://dx.doi.org/10.1203/PDR.0b013e318193f117.

[8] J. Beck, M. Reilly, G. Grasselli, H. Qui, A.S. Slutsky, M.S. Dunn, C.A. Sinderby, Characterization of neural breathing pattern in spontaneously breathing preterm infants, Pediatr. Res. 70 (6) (2011) 607–613, http://dx.doi.org/10.1203/PDR.0b013e318232100e.

[9] K. Fairchild, M. Mohr, A. Paget-Brown, C. Tabacaru, D. Lake, J. Delos, J.R. Moorman, J. Kattwinkel, Clinical associations of immature breathing in preterm infants: part 1—central apnea, Pediatr. Res. 80 (2016) 21–27, http://dx.doi.org/10.1038/pr.2016.43.

[10] M. Patel, M. Mohr, D. Lake, J. Delos, J.R. Moorman, R.A. Sinkin, J. Kattwinkel, K. Fairchild, Clinical associations with immature breathing in preterm infants: part 2—periodic breathing, Pediatr. Res. 80 (2016) 28–34, http://dx.doi.org/10.1038/pr.2016.58.

[11] A.H. Gee, R. Barbieri, D. Paydarfar, P. Indic, Predicting bradycardia in preterm infants using point process analysis of heart rate, IEEE Trans. Biomed. Eng. 64 (2017) 2300–2308, http://dx.doi.org/10.1109/TBME.2016.2632746.

[12] K. Lim, C. Eastwood-Sutherland, A.P. Marshall, T.J. Gale, P.A. Dargaville, Limitations of thoracic impedance monitoring for central apnoea detection in preterm infants, Acta Paediatr. 110 (2021) 2550–2552, http://dx.doi.org/10.1111/APA.15888.

[13] T. Niederhauser, A. Haeberlin, T. Marisa, M. Jungo, J. Goette, M. Jacomet, R. Abächerli, R. Vogel, Electrodes for Long-Term Esophageal Electrocardiography, IEEE Trans. Biomed. Eng. 60 (9) (2013) 2576–2584, http://dx.doi.org/10.1109/TBME.2013.2261067.

[14] P. Simmen, S. Kreuzer, M. Thomet, L. Suter, B. Jesacher, P.-A. Tran, A. Haeberlin, S. Schulzke, K. Jost, T. Niederhauser, Multichannel esophageal heart rate monitoring of preterm infants, IEEE Trans. Biomed. Eng. 68 (2021) 1903–1912, http://dx.doi.org/10.1109/TBME.2020.3030162.

[15] C. Bürgin, P. Simmen, N. Gupta, L. Suter, S. Kreuzer, A. Haeberlin, S.M. Schulzke, D. Trachsel, T. Niederhauser, K. Jost, Multichannel esophageal signals to monitor respiratory rate in preterm infants, Pediatr. Res. (2021) 1–9, http://dx.doi.org/10.1038/s41390-021-01748-4, 2021.

[16] P.H. Charlton, D.A. Birrenkott, T. Bonnici, M.A.F. Pimentel, A.E.W. Johnson, J. Alastruey, L. Tarassenko, P.J. Watkinson, R. Beale, D.A. Clifton, Breathing Rate Estimation From the Electrocardiogram and Photoplethysmogram: A Review, IEEE Rev. Biomed. Eng. 11 (2017) 2–20, http://dx.doi.org/10.1109/RBME.2017.2763681.

[17] J. Jorge, M. Villarroel, S. Chaichulee, G. Green, K. McCormick, L. Tarassenko, Assessment of signal processing methods for measuring the respiratory rate in the neonatal intensive care unit, IEEE J. Biomed. Health Inf. 23 (2019) 2335–2346, http://dx.doi.org/10.1109/JBHI.2019.2898273.

[18] P. Spincemaille, T.D. Nguyen, M.R. Prince, Y. Wang, Kalman filtering for real-time navigator processing, Magn. Reson. Med. 60 (1) (2008) 158–168, http://dx.doi.org/10.1002/mrm.21649.

[19] J. Foussier, D. Teichmann, J. Jia, B. Misgeld, S. Leonhardt, An adaptive Kalman filter approach for cardiorespiratory signal extraction and fusion of non-contacting sensors, BMC Med. Inform. Decis. Mak. 14 (2014) 1–15, http://dx.doi.org/10.1186/1472-6947-14-37, 2014 14:1.

[20] N.N. Lepine, T. Tajima, T. Ogasawara, R. Kasahara, H. Koizumi, Robust respiration rate estimation using adaptive Kalman filtering with textile ECG sensor and accelerometer, in: Proceedings of the Annual International Conference of the IEEE Engineering in Medicine and Biology Society, EMBS, 2016-October, Institute of Electrical and Electronics Engineers Inc., 2016, pp. 3797–3800, http://dx.doi.org/10.1109/EMBC.2016.7591555.

[21] S. Khreis, D. Ge, H.A. Rahman, G. Carrault, Breathing rate estimation using Kalman smoother with electrocardiogram and photoplethysmogram, IEEE Trans. Biomed. Eng. 67 (2020) 893–904, http://dx.doi.org/10.1109/TBME.2019.2923448.

[22] W. Karlen, CapnoBase IEEE TBME respiratory rate benchmark. http://dx.doi.org/10.5683/SP2/NLB8IT,

[23] Dryad | Data – Identification of thresholds for accuracy comparisons of heart rate and respiratory rate in neonates, 2023, [Online] URL https://datadryad.org/stash/dataset/doi:10.5061/dryad.1c59zw3vb. (Accessed 20 March 2023).

[24] B. Boashash, Estimating and interpreting the instantaneous frequency of a signal—Part 1: Fundamentals, Proc. IEEE 80 (1992) 520–538, http://dx.doi.org/10.1109/5.135376.

[25] B. Boashash, Estimating and interpreting the instantaneous frequency of a signal—Part 2: Algorithms and applications, Proc. IEEE 80 (1992) 540–568, http://dx.doi.org/10.1109/5.135378.

[26] J. Coleman, A.S. Ginsburg, W.M. Macharia, R. Ochieng, D. Chomba, G. Zhou, D. Dunsmuir, W. Karlen, J.M. Ansermino, Assessment of neonatal respiratory rate variability, J. Clin. Monit. Comput. 36 (6) (2022) 1869–1879, http://dx.doi.org/10.1007/s10877-022-00840-2, arXiv:35332406.

[27] M. Elgendi, M. Jonkman, F. DeBoer, Heart Rate Variability and the Acceleration Plethysmogram Signals Measured at Rest, in: Biomedical Engineering Systems and Technologies, Springer, 2011, pp. 266–277, http://dx.doi.org/10.1007/978-3-642-18472-7_21.

[28] J. Lázaro, E. Gil, J.M. Vergara, P. Laguna, Pulse Rate Variability Analysis for Discrimination of Sleep-Apnea-Related Decreases in the Amplitude Fluctuations of Pulse Photoplethysmographic Signal in Children, IEEE J. Biomed. Health Inf. 18 (1) (2013) 240–246, http://dx.doi.org/10.1109/JBHI.2013.2267096.

[29] S. Nemati, A. Malhotra, G.D. Clifford, Data Fusion for Improved Respiration Rate Estimation, EURASIP J. Adv. Signal Process. 2010 (2010) 926305, http://dx.doi.org/10.1155/2010/926305.

[30] M.A.F. Pimentel, A.E.W. Johnson, P.H. Charlton, D. Birrenkott, P.J. Watkinson, L. Tarassenko, D.A. Clifton, Toward a Robust Estimation of Respiratory Rate From Pulse Oximeters, IEEE Trans. Biomed. Eng. 64 (8) (2017) 1914, http://dx.doi.org/10.1109/TBME.2016.2613124.

[31] W. Karlen, J.M. Ansermino, G. Dumont, Adaptive pulse segmentation and artifact detection in photoplethysmography for mobile applications, in: 2012 Annual International Conference of the IEEE Engineering in Medicine and Biology Society, IEEE, 2012, pp. 3131–3134, http://dx.doi.org/10.1109/EMBC.2012.6346628.

[32] W. Karlen, S. Raman, J.M. Ansermino, G.A. Dumont, Multiparameter respiratory rate estimation from the photoplethysmogram, IEEE Trans. Biomed. Eng. 60 (2013) 1946–1953, http://dx.doi.org/10.1109/TBME.2013.2246160.

[33] J. Pan, W.J. Tompkins, A real-time QRS detection algorithm, IEEE Trans. Biomed. Eng. 32 (3) (1985) 230–236, http://dx.doi.org/10.1109/TBME.1985.325532.

[34] M.J. Tadi, E. Lehtonen, T. Hurnanen, J. Koskinen, J. Eriksson, M. Pänkäälä, M. Teräs, T. Koivisto, A real-time approach for heart rate monitoring using a Hilbert transform in seismocardiograms, Physiol. Meas. 37 (11) (2016) 1885, http://dx.doi.org/10.1088/0967-3334/37/11/1885.

[35] J.E. Hernandez, E. Cretu, A wireless, real-time respiratory effort and body position monitoring system for sleep, Biomed. Signal Process. Control 61 (2020) 102023, http://dx.doi.org/10.1016/j.bspc.2020.102023.

[36] P. Hamelmann, R. Vullings, M. Mischi, A.F. Kolen, L. Schmitt, J.W.M. Bergmans, An Extended Kalman Filter for Fetal Heart Location Estimation During Doppler-Based Heart Rate Monitoring, IEEE Trans. Instrum. Meas. 68 (9) (2018) 3221–3231, http://dx.doi.org/10.1109/TIM.2018.2876779.